Original Article

Assessment of rhabdomyolysis-induced acute kidney injury with chemical exchange saturation transfer magnetic resonance imaging

Qianqian Zhang[1,2#^], Quan Tao[2,3#^], Yuanyao Xie[1,2^], Zelong Chen[4^], Erdmann Seeliger[5^], Thoralf Niendorf[6^], Wufan Chen[1,2*^], Yanqiu Feng[1,2,7,8*]

[1]School of Biomedical Engineering, Southern Medical University, Guangzhou, China; [2]Guangdong Provincial Key Laboratory of Medical Image Processing & Guangdong Province Engineering Laboratory for Medical Imaging and Diagnostic Technology, Southern Medical University, Guangzhou, China; [3]Department of Rehabilitation, Zhujiang Hospital, Southern Medical University, Guangzhou, China; [4]Medical Imaging Center, Nanfang Hospital, Southern Medical University, Guangzhou, China; [5]Institute of Translational Physiology, Charite-Universitatsmedizin Berlin, Berlin, Germany; [6]Berlin Ultrahigh Field Facility (B.U.F.F.), Max Delbruck Center for Molecular Medicine in the Helmholtz Association, Berlin, Germany; [7]Department of Radiology, Shunde Hospital, Southern Medical University (The First People's Hospital of Shunde, Foshan), Foshan, China; [8]Key Laboratory of Mental Health of the Ministry of Education & Guangdong-Hong Kong-Macao Greater Bay Area Center for Brain Science and Brain-Inspired Intelligence, Southern Medical University, Guangzhou, China

Contributions: (I) Conception and design: Q Zhang, Q Tao, Y Feng; (II) Administrative support: Y Feng, W Chen; (III) Provision of study materials or patients: Q Zhang, Q Tao; (IV) Collection and assembly of data: Q Zhang, Q Tao, Y Xie; (V) Data analysis and interpretation: Q Zhang, Q Tao, Z Chen, Y Xie, E Seeliger, T Niendorf; (VI) Manuscript writing: All authors; (VII) Final approval of manuscript: All authors.

[#]These authors contributed equally to this work.

*These authors contributed equally to this work as co-corresponding authors.

Correspondence to: Yanqiu Feng, PhD. School of Biomedical Engineering, Southern Medical University, No. 1023, Shatai Road, Baiyun District, Guangzhou 510515, China; Guangdong Provincial Key Laboratory of Medical Image Processing & Guangdong Province Engineering Laboratory for Medical Imaging and Diagnostic Technology, Southern Medical University, Guangzhou, China; Department of Radiology, Shunde Hospital, Southern Medical University (The First People's Hospital of Shunde, Foshan), Foshan, China; Key Laboratory of Mental Health of the Ministry of Education & Guangdong-Hong Kong-Macao Greater Bay Area Center for Brain Science and Brain-Inspired Intelligence, Southern Medical University, Guangzhou, China. Email: foree@163.com; Wufan Chen, PhD. School of Biomedical Engineering, Southern Medical University, No. 1023, Shatai Road, Baiyun District, Guangzhou 510515, China; Guangdong Provincial Key Laboratory of Medical Image Processing & Guangdong Province Engineering Laboratory for Medical Imaging and Diagnostic Technology, Southern Medical University, Guangzhou, China. Email: chenwf@smu.edu.cn.

Background: Rhabdomyolysis (RM)-induced acute kidney injury (AKI) is a common renal disease with low survival rate and inadequate prognosis. In this study, we investigate the feasibility of chemical exchange saturation transfer (CEST) magnetic resonance imaging (MRI) for assessing the progression of RM-induced AKI in a mouse model.

Methods: AKI was induced in C57BL/6J mice via intramuscular injection of 7.5 mL/kg glycerol (n=30). Subsequently, serum creatinine (SCr), blood urea nitrogen (BUN), and hematoxylin-eosin (HE) and Masson staining, were performed. Longitudinal CEST-MRI was conducted on days 1, 3, 7, 15, and 30 after AKI induction using a 7.0-T MRI system. CEST-MRI quantification parameters including magnetization transfer

^ ORCID: Qianqian Zhang, 0009-0008-3107-2839; Quan Tao, 0009-0006-6354-6811; Yuanyao Xie, 0000-0002-6781-5971; Zelong Chen, 0000-0002-0447-7055; Erdmann Seeliger, 0000-0002-5685-8044; Thoralf Niendorf, 0000-0001-7584-6527; Wufan Chen, 0000-0002-4125-7537.

ratio (MTR), MTR asymmetric analysis (MTR_{asym}), apparent amide proton transfer (APT*), and apparent relayed nuclear Overhauser effect (rNOE*) were used to investigate the feasibility of detecting RM-induced renal damage.

Results: Significant increases of SCr and BUN demonstrated established AKI. The HE staining revealed various degrees of tubular damage, and Masson staining indicted an increase in the degree of fibrosis in the injured kidneys. Among CEST parameters, the cortical MTR presented a significant difference, and it also showed the best diagnostic performance for AKI [area under the receiver operating characteristic curve (AUC) =0.915] and moderate negative correlations with SCr and BUN. On the first day of renal damage, MTR was significantly reduced in cortex (22.7%±0.04%, P=0.013), outer stripe of outer medulla (24.7%±1.6%, P<0.001), and inner stripe of outer medulla (27.0%±1.5%, P<0.001) compared to the control group. Longitudinally, MTR increased steadily with AKI progression.

Conclusions: The MTR obtained from CEST-MRI is sensitive to the pathological changes in RM-induced AKI, indicating its potential clinical utility for the assessment of kidney diseases.

Keywords: Magnetic resonance imaging (MRI); chemical exchange saturation transfer (CEST); rhabdomyolysis (RM); acute kidney injury (AKI)

Submitted May 18, 2023. Accepted for publication Sep 26, 2023. Published online Oct 19, 2023.
doi: 10.21037/qims-23-699
View this article at: https://dx.doi.org/10.21037/qims-23-699

Introduction

Rhabdomyolysis (RM) is a medical condition involving rapid destruction of skeletal muscles induced by physical or chemical damage (1), such as physical trauma, drug toxicity, infections, and physical exertion (2,3). Acute kidney injury (AKI) is one of the most severe complications (with an incidence rate of 15–50%) in RM patients (4,5), and accounts for approximately 7–10% of all cases of acute renal failure (6). RM-induced AKI is associated with the prolonged stay of patients in intensive care units and can lead to a mortality rate of up to 37% (7). Therefore, early diagnosis and long-term evaluation of RM-induced AKI are crucial for effective disease management and therapeutic intervention.

Currently, measurement of blood urea nitrogen (BUN) and serum creatinine (SCr) are regularly performed to clinically assess kidney injury. Although quick and economical, their sensitivity is rather low as they only detect reductions in glomerular filtration rate (8-10). Renal biopsy is the gold standard for definitive diagnosis, but it is invasive and associated with risks such as bleeding and infection, and subject to sampling bias (11).

Magnetic resonance imaging (MRI) techniques have been employed for the noninvasive assessment of renal disorders (12). In addition to the measurement of renal morphology (13,14), MRI facilitates the assessment of various functional features. Blood oxygen level-dependent MRI is sensitive to intrarenal oxygenation (15,16), the MRI of water diffusion is sensitive to renal fibrosis (17,18), and arterial spin labeling assesses renal blood perfusion (19). Dynamic contrast-enhanced MRI can be used to assess changes in renal perfusion and the permeability of the blood vessels (20,21). However, these MRI techniques do not provide information on metabolites.

Chemical exchange saturation transfer (CEST) is an emerging molecular MRI technology. After irradiation by radio frequency (RF) pulses, saturated protons in biomolecules are exchanged with water protons, resulting in a detectable reduction of the water signal. This technique is sensitive to the concentration and the exchange rate of endogenous metabolites, and their environment (22,23). Exogenous CEST can detect pH changes using pH-responsive clinically approved iodinated contrast agents (24,25) in RM-induced AKI (26), ischemia-reperfusion (27), and unilateral ureteral obstruction (28). Endogenous CEST contrast includes amides (on proteins), amines (on glutamate and creatine), and hydroxyl proton (on glucose and glycogen). It has been shown that the CEST signal of hydroxyl protons facilitates the monitoring of the progression of diabetic nephropathy (29), and that the amide transfer signal changes significantly in early sepsis-induced AKI (30).

This study aimed to investigate the feasibility of using CEST-MRI to assess renal injury and the progression of RM-induced AKI. For this purpose, we established a RM-induced AKI mouse model using intramuscular glycerol injection and performed longitudinal renal CEST-MRI. Amide proton transfer (APT) and relayed nuclear Overhauser enhancement (rNOE) effects were quantified based on the CEST-MRI signals using the magnetization transfer ratio (MTR), MTR asymmetric analysis (MTR_{asym}), and the 3-point method. These metrics were correlated with animal characteristics, blood parameters, and histologic assessments. We also evaluated the diagnostic performance of quantitative CEST parameters in the detection of RM-induced renal injury.

Methods

Animals

Experiments were performed under a project license (No. 2016-0167) granted by Institutional Animal Care and Use Committee of Southern Medical University, in compliance with Southern Medical University institutional guidelines for the care and use of animals. Male mice were used in the experiments, and all the mice were kept in a 12/12 h light-dark cycle environment with adequate chow and water. Before induction of RM, the mice were deprived of water for 12 hours (25). All C57BL/6J mice (8–10 weeks old) were anesthetized using isoflurane (1–2%) and randomly assigned to either an AKI group or a healthy control group. Each mouse was weighed before injection. The AKI group received a bilateral intramuscular injection of 50% glycerol solution (7.5 mL/kg body weight, n=30), whereas the control group was administered the same volume of 0.9% normal saline (n=10). Mice were longitudinally weighed and imaged on days 1, 3, 7, 15, and 30 after injection.

Blood testing and histology examination

Blood and kidney specimens were collected from euthanized mice. Serum was obtained from supernatant liquid after extracted blood was centrifuged at 3,500 rpm for 12 minutes at 4 ℃. SCr and BUN levels were measured using an automatic biochemical analyzer. To measure the kidney water content, the right kidney was dried to a constant weight in an oven at 60 ℃. Paraffin tissue sections were processed from the left kidney using standard procedures. The kidney sections were stained using hematoxylin-eosin (HE) and Masson. Renal histological analysis and collagen deposition was assessed by 2 experienced nephropathologists who were blinded to the animal's group identity.

In vivo MRI studies

All MRI experiments were conducted using a 7.0-T animal MRI scanner (Bruker BioSpec, Ettlingen, Germany) equipped with a 40 mm volume RF coil (transmission) and a 4-channel phased array surface RF coil (reception). For the MRI examination, each mouse was anesthetized (isoflurane 1–2%) and immobilized on a heated animal bed maintained at 37 ℃. Respiratory gating was used to continuously monitor the respiration and to synchronize data acquisition with the respiratory cycle to suppress breathing artifacts, maintaining a rate of 60±2 respiration cycles per minute by controlling the flow (L/min) of gas (air and isoflurane). All imaging protocols used a single coronal slice with a field of view (FOV) of 30×30 mm^2. The coronal slice was positioned near the center of the kidney with the largest cross-section on both kidneys by using the sagittal and axial scout images. For correct delineation of regions of interest (ROIs) in the kidney, T_2-weighted images were acquired using 2-dimensional (2D) rapid acquisition with relaxation enhancement (RARE) [repetition time (TR) =2.5 s, effective echo time (TE) =60 ms, slice thickness =1 mm, matrix size =256×256, RARE factor =16, number of averages (NA) =2, and total acquisition time =100 s].

CEST-MRI was conducted using a modified 2D RARE variant with a continuous-wave pre-saturation RF pulse: duration of saturation pulse =3 s, saturation power (B_1) =1.5 μT, TR =6 s, effective TE =3.6 ms, matrix size =90×90, RARE factor =36, partial Fourier in phase direction=1.8, NA =2. Fat-suppression was applied with a frequency-selective saturation pulse at a frequency offset of −3.5 ppm relative to the water. Saturation images were obtained at 53 frequency offsets ($\Delta\omega$ =−10.0, −9.0, −8.0, −7.0, −6.0, −5.0, −4.4, −4.2, −4.0, −3.8, −3.6, −3.4, −3.2, −3.0, −2.5, −2.0, −1.8, −1.6, −1.4, −1.2, −1.0, −0.8, −0.6, −0.4, −0.2, −0.1, 0, 0.1, 0.2, 0.4, 0.6, 0.8, 1.0, 1.2, 1.4, 1.6, 1.8, 2.0, 2.5, 3.0, 3.2, 3.4, 3.6, 3.8, 4.0, 4.2, 4.4, 5.0, 6.0, 7.0, 8.0, 9.0, 10.0 ppm). An unsaturated image was obtained at 100 ppm. The total acquisition time was 11 minutes 48 seconds. To correct for B_0 inhomogeneity, water saturation shift referencing (WASSR) data (31) were acquired using B_1 =0.3 μT and

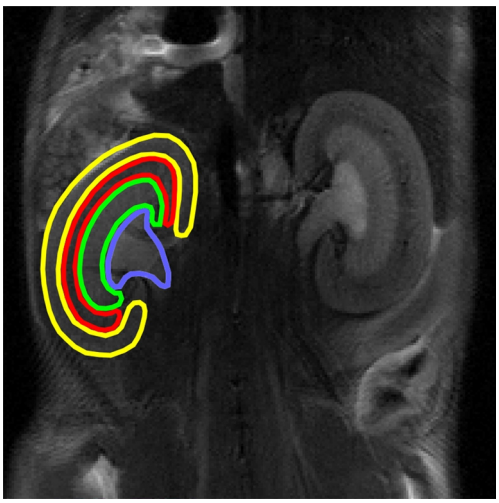

Figure 1 Placement of ROIs on T2-weighted images obtained from MRI. For ROI placement four anatomical layers of kidney, cortex (yellow), OSOM (red), ISOM (green), and IM + P (blue) were used. ROI, region of interest; MRI, magnetic resonance imaging; OSOM, outer stripe of outer medulla; ISOM, inner stripe of outer medulla; IM + P, inner medulla and pelvis.

intervals of 0.02 ppm to cover a range of ±0.5 ppm.

Data processing

All data were processed using MATLAB (MathWorks, Natick, MA, USA). The weight of each mouse was recorded prior to euthanasia. The organ index of the kidney was calculated as follows:

$$\text{Organ index of kidney} = \frac{\text{Weight of kidneys}(\text{g})}{\text{Body weight}(\text{g})} \quad [1]$$

The Z-spectra were B_0-corrected using WASSR and normalized to the control scan, and spline interpolation was applied for accurate quantification. The MTR was obtained as follows:

$$\text{MTR}(3.6\ \text{ppm}) = 1 - \frac{S_{sat}(3.6\ \text{ppm})}{S_0} \quad [2]$$

where $\Delta\omega$ is the offset frequency of the applied RF pulses with respect to water peak, S_{sat} ($\pm\Delta\omega$) is the water saturation signal intensity obtained at $\pm\Delta\omega$, and S_0 is the unsaturated water signal intensity. The conventional MTR_{asym} was calculated as follows:

$$\text{MTR}_{asym}(3.6\ \text{ppm}) = \frac{S_{sat}(-3.6\ \text{ppm})}{S_0} - \frac{S_{sat}(3.6\ \text{ppm})}{S_0} \quad [3]$$

The apparent APT (APT*) and apparent rNOE (rNOE*) were calculated using the 3-point method (29). APT* maps were calculated from label image collected at 3.6 ppm and 2 boundary images acquired at 3.0 and 4.2 ppm with:

$$\text{APT}^* = \frac{\frac{S_{sat}(3.0\ \text{ppm})}{S_0} + \frac{S_{sat}(4.2\ \text{ppm})}{S_0}}{2} - \frac{S_{sat}(3.6\ \text{ppm})}{S_0} \quad [4]$$

rNOE* maps were obtained similarly from three images acquired at −5.0, −2.0, and −3.6 ppm with:

$$\text{rNOE}^* = \frac{\frac{S_{sat}(-2.0\ \text{ppm})}{S_0} + \frac{S_{sat}(-5.0\ \text{ppm})}{S_0}}{2} - \frac{S_{sat}(-3.6\ \text{ppm})}{S_0} \quad [5]$$

High-resolution T_2-weighted images were used to delineate ROIs including the cortex, the outer stripe of the outer medulla (OSOM), the inner stripe of the outer medulla (ISOM), and the inner medulla and pelvis (IM + P) for regional data analyses (*Figure 1*). The IM + P were integrated for regional quantification because of the difficulty in separating them, especially in the AKI groups. These ROIs were applied to all the maps to determine the averaged values corresponding to the renal layers.

Statistical analysis

For statistical analysis, GraphPad Prism 8 software (GraphPad Software, La Jolla, CA, USA) and MedCalc (MedCalc Software, Ostend, Belgium) were used. The data were expressed as the mean ± standard deviation. An unpaired, two-tailed Student's *t*-test was used to compare the difference between control and AKI groups. Pearson correlation coefficients were obtained for comparisons between the CEST parameters, physiologic characteristics, blood parameters, and fibrosis score. Receiver operating characteristic (ROC) curve analysis was used to compare diagnostic performance. The area under the ROC curve (AUC) was compared using DeLong's method (32) and the Youden index (33) was used to calculate sensitivity and specificity for the detection of AKI at the optimal threshold value. We used *P<0.05, **P<0.01, ***P<0.001,

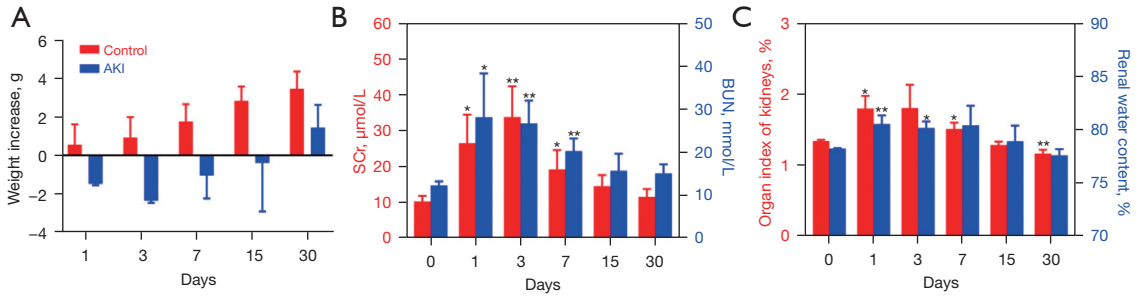

Figure 2 Animal characteristics and blood assessment of injured kidneys. Changes in (A) control (red) and AKI (blue) mice body weight over time, (B) blood SCr (red) and BUN (blue) levels over time, (C) organ index of kidneys (red) and mono-renal water content (blue) over time. The number of mice in the control group and AKI group at each time point was 5 and 6, respectively. *, P<0.05; **, P<0.01 in comparison to day 0 values. AKI, acute kidney injury; SCr, serum creatinine; BUN, blood urea nitrogen.

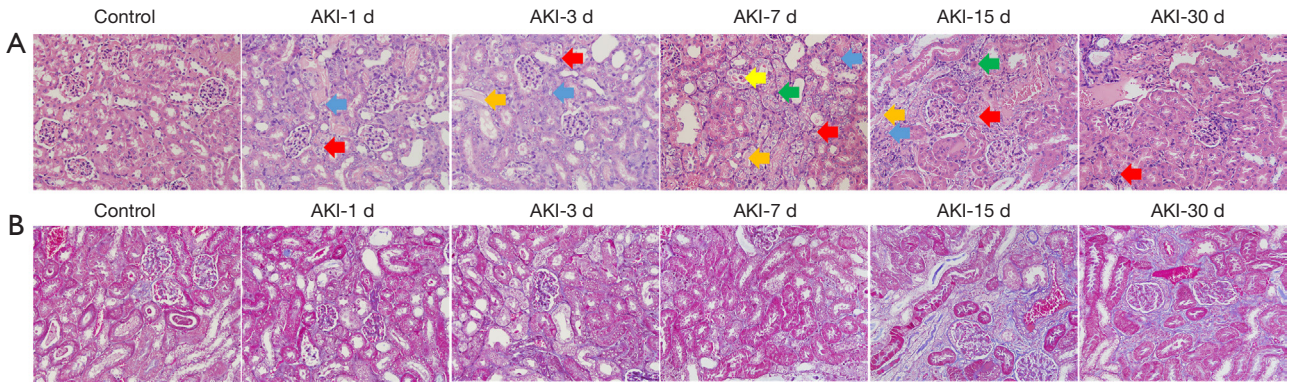

Figure 3 Animal histologic assessment of injured kidneys. HE (A) and Masson (B) stains (×400) of representative control and AKI mice. Red arrows indicate moderate-to-severe edema. Blue arrows indicate enlarged nuclei of tubular cells. Yellow arrows indicate exfoliated cells visible in lumen. Green arrows indicate eosinophilic change. Orange arrows indicate transparent tube type formation. HE, hematoxylin-eosin; AKI, acute kidney injury.

and ****P<0.0001 to represent the degree of statistical significance.

Results

Animal characteristics, blood parameters, and histologic assessment

The results for the body weight, SCr, BUN, and histology are shown in *Figure 2* and *Figure 3*. The body weight of the AKI mice decreased during the first 3 days after glycerol injection, then gradually increased, whereas the control mice steadily gained weight (*Figure 2A*). The BUN and SCr levels were increased significantly from day 1 to day 7 after glycerol injection. Thereafter, it gradually returned to physiological values (*Figure 2B*). The organ index of the kidney and renal water content exhibited similar trends to the SCr and BUN (*Figure 2C*).

The results of the histologic assessments of the HE- and Masson-stained renal sections are shown in *Figure 3A,3B*. Tubular epithelium edema (red arrows), large tubular epithelial nuclei (blue arrows), eosinophilic changes (green arrows), and hyaline tubular patterns (orange arrows) were observed in the HE-stained samples of the injured kidneys during the period of days 3–15. Cellular shedding was occasionally observed in the lumen (yellow arrows). The purple region of the Masson-stained sections was enlarged with the progression of AKI, corresponding to fibrosis scores obtained on day 1, 3, 7, 15 and 30 of 1, 1, 1, 2, and 2, respectively. These scores confirmed the increase in collagen deposition and interstitial fibrosis.

CEST-MRI for RM-induced AKI

Figure 4 shows the Z-spectra and CEST images at different time points. The Z-spectra of the entire kidney are smooth and without the apparent fluctuations caused by respiratory motion (*Figure 4A*). There were substantial signal reductions at frequency offsets of 3.6 and –3.6 ppm, which indicated the feasibility of reliable APT and rNOE signal quantification, respectively. Representative MTR, MTR_{asym}, APT*, and rNOE* maps acquired for the control and the AKI mice are shown in *Figure 4B*. The renal structure was distinct in various maps of the control group, but was lost after the injury progressed. Injured kidneys exhibited a lower MTR signal, whereas the MTR_{asym} increased. The APT* and rNOE* images did not exhibit overt changes.

Figure 5 summarizes the results derived from MTR, MTR_{asym}, APT*, and rNOE* quantification in cortex, OSOM, ISOM, and IM + P. After AKI induction, the MTR decreased significantly and reached the lowest value at day 1 in cortex (22.7%±0.04%, P=0.013), OSOM (24.7%±1.6%, P<0.001), and ISOM (27.0%±1.5%, P<0.001). The most pronounced MTR changes (–19.5% compared to control) occurred in cortex at day 1. Subsequently, the MTR exhibited recovery without a significant difference compared to the control group at day 30. *Figure 5B* demonstrates that the MTR_{asym} increased significantly with AKI progression, and reached a maximum at day 7 in ISOM (–3.2%±2.0%, P=0.02), and day 15 in cortex (–6.1%±2.3%, P<0.001) and OSOM (–6.1%±3.1%, P=0.02). The largest MTR_{asym} changes (–51.1% compared to the control) occurred in cortex at day 1. *Figure 5C* shows that APT* increased significantly at day 3 in cortex (1.4%±0.3%, P=0.006), and at day 7 in OSOM (1.5%±0.3%, P=0.031). The APT* obtained in cortex was significantly reduced at day 30 (0.5%±0.2%, P<0.001), and the APT* of ISOM (1.1%±0.2%, P=0.006) and IM + P (0.9%±0.3%, P=0.002) also showed a significant decrease at day 30 compared to the control group. *Figure 5D* demonstrates that rNOE* decreased in injured kidneys, and reached a minimum at day 7. However, there is no significant difference when compared to the control group.

Correlation between CEST parameters, animal characteristics, blood parameters, and histology

Figure 6 shows the Pearson correlation between various cortical CEST parameters (including MTR, MTR_{asym}, APT*, and rNOE*), organ index of kidney, renal water content, BUN/SCr levels, and fibrosis score. Moderately negative correlations were obtained between MTR and SCr (r=–0.59, P<0.01), and BUN (r=–0.57, P<0.01). MTR_{asym} showed weak positive correlations with SCr (r=0.48, P=0.02). Weak negative correlations were obtained between APT* and fibrosis (r=–0.41, P=0.04), and moderately negative correlations were obtained between rNOE* and fibrosis (r=0.53, P=0.01). The correlation results for ISOM, OSOM, and IM + P are shown in Figure S1. The Pearson correlations between the CEST-MRI signal and the blood parameters for ISOM and OSOM were similar to that obtained for cortex, with ISOM exhibiting the highest correlation. For example, there was a stronger correlation between MTR and SCr for ISOM (r=–0.62, P<0.01) than for OSOM (r=–0.43, P=0.04) (Figure S1). Considering the metrics obtained from CEST-MTR, MTR showed the strongest correlation with pathological changes (especially in BUN and SC) for RM-induced AKI.

Diagnostic performance in differentiating between healthy and damaged kidneys

The results of the ROC curve analysis for RM-induced AKI diagnosis are shown in *Table 1*. MTR exhibited the best diagnostic performance in cortex (AUC =0.915), OSOM (AUC =0.885), and ISOM (AUC =0.883). However, the CEST parameters could not be used to detect renal damage in IM + P. These results indicate that CEST-MRI is suitable for the detection of renal injury induced by RM.

Discussion

CEST-MRI is sensitive to the exchangeable proton concentration and the exchange rate, and is a promising technique for the detection of pathophysiological changes in an intrarenal environment and endogenous metabolite concentrations. Our work contributes to the literature by investigating the application of CEST-MRI for the assessment of RM-induced AKI. Our results demonstrate that MTR decreased significantly in AKI on day 1, followed by a steady increase with AKI development. This observation indicates that MTR-CEST is a sensitive surrogate for the detection of renal injury during the acute stage of RM injury and for the assessment of its progression during the recovery stage.

Interpretation of CEST signal changes

We observed substantial APT and rNOE effects related

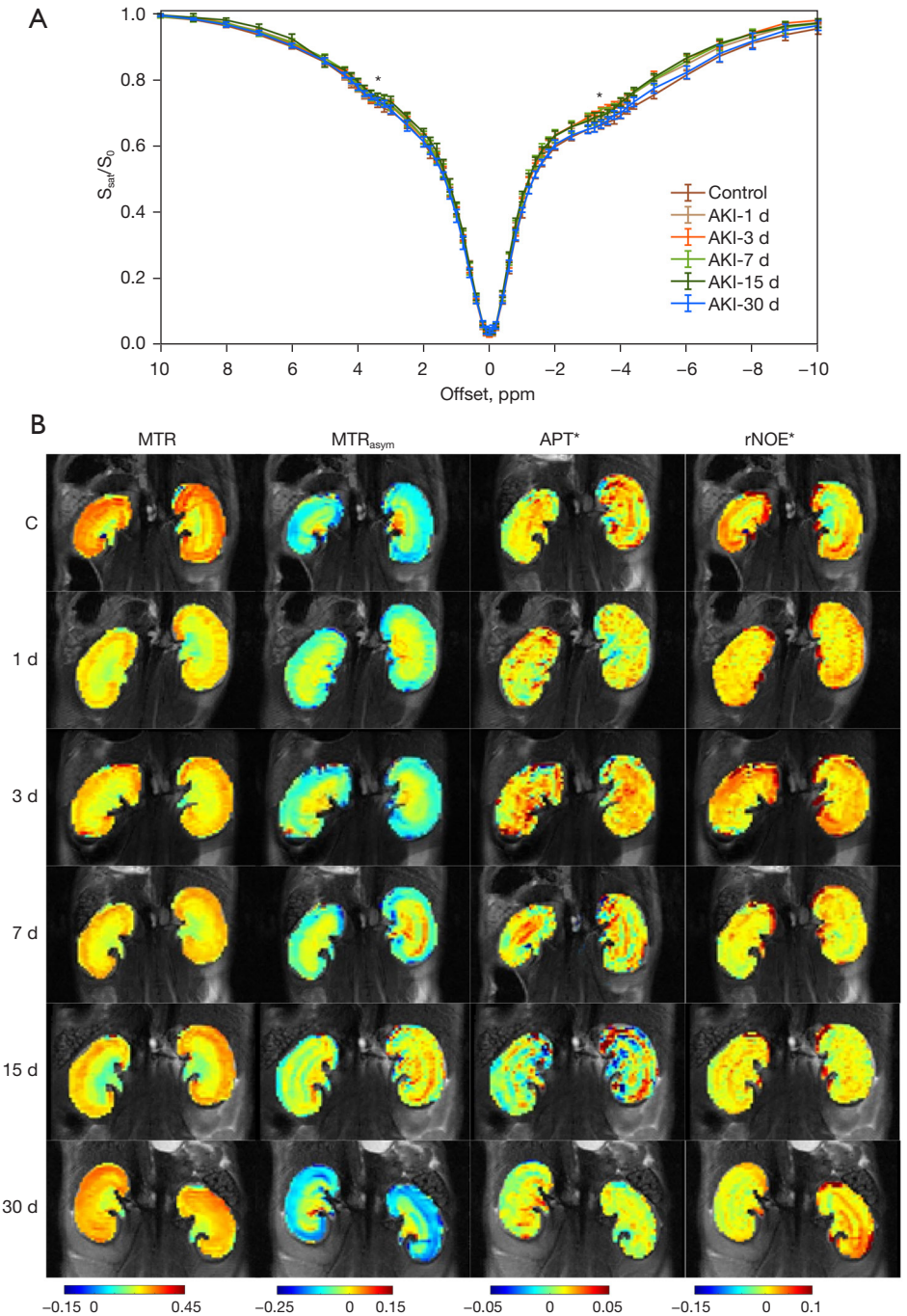

Figure 4 Z-spectral analysis and CEST images of control and AKI kidneys. (A) Renal Z-spectral for all mice. Asterisks indicate CEST effects. (B) Longitudinal comparison of renal MTR (3.6 ppm) (first column), MTR_{asym} (3.6 ppm) (second column), APT* (third column), rNOE* (last column) maps in representative mice. S_{sat}, water saturation signal intensity; S_0, unsaturated water signal intensity; AKI, acute kidney injury; MTR, magnetization transfer ratio; MTR_{asym}, asymmetric MTR; APT*, apparent amide proton transfer; rNOE*, apparent relayed nuclear Overhauser enhancement; CEST, chemical exchange saturation transfer.

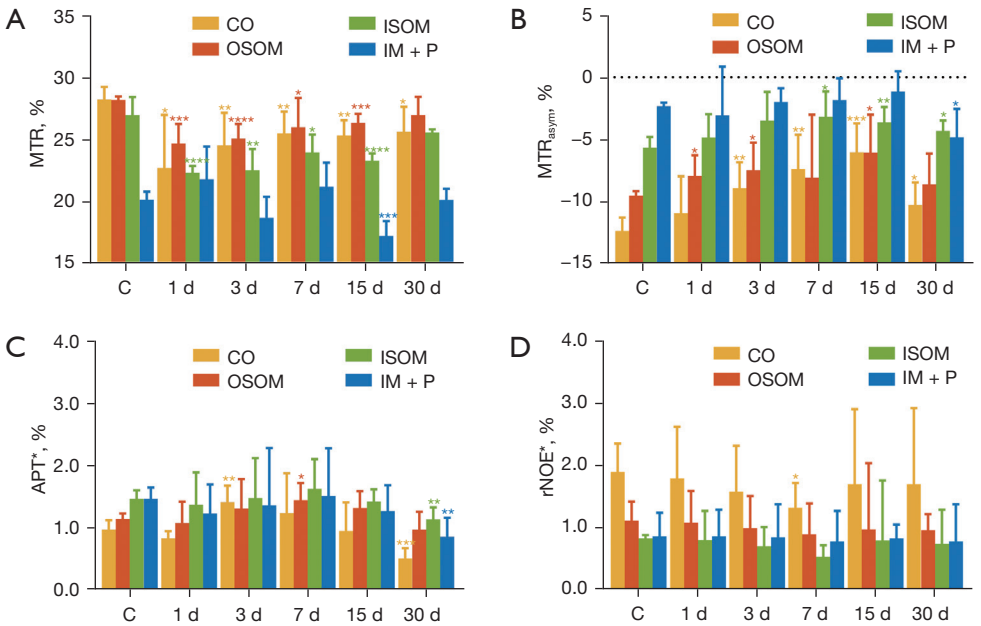

Figure 5 Summary of metrics obtained from renal CEST-MRI after AKI. Time course obtained for MTR (3.6 ppm) (A), MTR_{asym} (3.6 ppm) (B) and for the three-point method including APT* (C) and rNOE* (D) for renal ROIs. The number of mice in the control group and AKI group at each time point was 5 and 6, respectively. Significant differences obtained for rhabdomyolysis-induced AKI compared to control group are indicated by *, P<0.05; **, P<0.01; ***, P<0.001; and ****, P<0.0001. MTR, magnetization transfer ratio; CO, cortex; ISOM, inner stripe of outer medulla; OSOM, outer stripe of outer medulla; IM + P, inner medulla and pelvis; C, control group; MTR_{asym}, asymmetric MTR; APT*, apparent amide proton transfer; rNOE*, apparent relayed nuclear Overhauser enhancement; CEST, chemical exchange saturation transfer; MRI, magnetic resonance imaging; AKI, acute kidney injury; ROIs, regions of interest.

to renal injury at ±3.6 ppm in the Z-spectra derived from the AKI.

The main factors that contribute to APT changes include mobile protein and peptide concentrations (23) and *in vivo* pH (25,34). First, owing to the base catalysis of *in vivo* amide protons, a low pH leads to a decrease in APT (35). It was determined in a previous study that the pH increases, peaks at day 3, and subsequently recovers at day 21 in glycerol-induced AKI mice (25). Consequently, pH variation may contribute to the changes in APT contrast during RM-induced AKI progression. Second, an increase in the water content, related to the edema caused by inflammation leads to a decrease in protein concentration and APT signal reduction (36). Inflammation was evident in the RM-induced AKI model (37). Based on the experiments, it was determined that the water content increased significantly during days 1–3 and gradually recovered thereafter. This finding suggests that water content changes may affect APT signals during AKI progression. Third, apoptosis of tubular epithelial cells occurs in RM-induced renal injury (37), which induces cell lysis that alters the concentration of macromolecules in the renal microstructure. As such, cell apoptosis might also contribute to the reduction of APT. Thus, the APT-weighted contrast at +3.6 ppm might be primarily influenced by edema, apoptosis, and pH.

The origin of the signal obtained at −3.6 ppm in the renal Z-spectra is complex and challenging to interpret (38). Based on previous studies, the decrease in the signal at −3.6 ppm was generally attributed to rNOE effects, which originated from membrane lipids and mobile macromolecules (lipoproteins) (39-41). In our study, a fat suppression technique was used to exclude the effect of lipids on rNOE. Second, blood contains plentiful albumin and hemoglobin with side-chain aliphatic protons, and was determined to have a large rNOE signal (35). RM leads to a large release of myoglobin that indirectly induces vasoconstriction and by reduces blood flow (36). This may explain the decrease in the rNOE signal in our study.

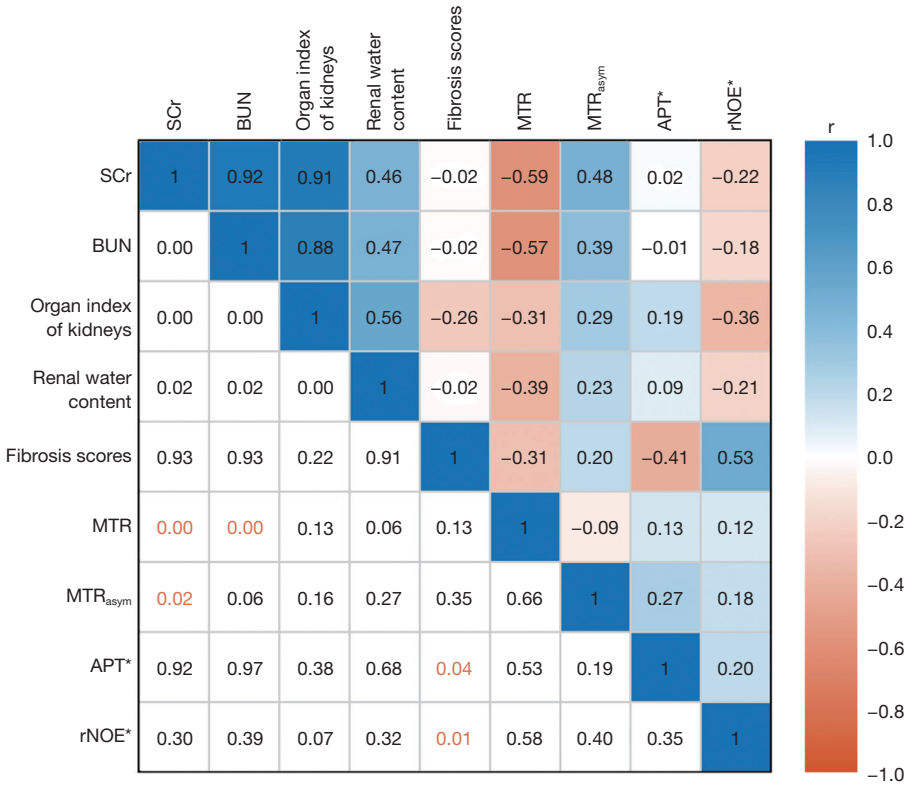

Figure 6 Pearson correlations between cortical changes obtained from CEST-MRI [MTR (3.6 ppm), MTR_{asym} (3.6 ppm), APT* and rNOE*] and animal characteristics, blood indexes, and histology. The lower triangle represents P values, and the upper triangle represents correlation coefficients. SCr, serum creatinine; BUN, blood urea nitrogen; MTR, magnetization transfer ratio; APT*, apparent amide proton transfer; rNOE*, apparent relayed nuclear Overhauser enhancement; CEST, chemical exchange saturation transfer; MRI, magnetic resonance imaging.

Third, apoptosis also leads to cell membrane rupturing, and discharge of their phospholipids, which then decreases the rNOE signal (41). Overall, the changes in the rNOE signal at –3.6 ppm observed in this study might be primarily influenced by apoptosis and renal blood flow.

Comparison of multiple CEST quantitative parameters

Various quantification methods for the Z-spectra obtained from CEST-MRI can generate quantitative metrics. We quantified 4 parameters including MTR, MTR_{asym}, APT*, and rNOE*. MTR_{asym} is susceptible to B_0-inhomogeneity and rNOE effects (42). Our finding that rNOE effects significantly change in injured kidneys may conflict with the use of MTR_{asym} as a metric to assess CEST effects. APT* and rNOE* were determined using the 3-point method, which is highly specific and can minimize the effect associated with magnetization transfer contrast and direct water saturation (43). However, the APT and rNOE signals were broadened in our study, causing an underestimation of the APT* and rNOE* parameters. MTR primarily combines magnetization transfer and APT effects without rNOE effects (44). In our study, MTR in cortex and the outer medulla exhibited a distinct decrease at day 1, and thus may be more sensitive than the increase in BUN and SCr, which peaked only at day 3. Following the initial decrease, MTR gradually increased with the stage of fibrosis. This observation concurs with the finding that renal fibrosis detected via MTR is consistent with the results of renal Sirius-red staining sections (45). Therefore, MTR can be considered a reliable parameter for detecting renal injury and assessing the progression of RM-induced AKI.

Potential of the transition from animal models to patients

The glycerol-based animal model is a relatively well-

Table 1 Results of the ROC curve analysis to evaluate the feasibility of the CEST-MRI parameters for detecting AKI in different renal layers

Parameters	AUC	95% CI	Sensitivity (%)	Specificity (%)	P value
CO					
MTR	0.915	0.783–0.980	73.33	100.00	<0.0001
MTR_{asym}	0.863	0.718–0.951	73.33	90.00	<0.0001
APT*	0.523	0.360–0.683	70.00	0	0.8032
rNOE*	0.667	0.478–0.856	66.67	83.33	0.2029
OSOM					
MTR	0.885	0.744–0.964	70.00	100.00	<0.0001
MTR_{asym}	0.783	0.625–0.898	70.00	100.00	0.0001
APT*	0.612	0.445–0.761	50.00	90.00	0.2027
rNOE*	0.575	0.354–0.797	56.67	66.67	0.5666
ISOM					
MTR	0.883	0.742–0.963	63.33	100.00	<0.0001
MTR_{asym}	0.840	0.690–0.936	70.00	100.00	<0.0001
APT*	0.503	0.341–0.665	83.33	0	0.9739
rNOE*	0.598	0.423–0.773	51.72	100.00	0.4568
IM + P					
MTR	0.593	0.427–0.746	40.00	100.00	0.3037
MTR_{asym}	0.582	0.415–0.735	60.00	80.00	0.3576
APT*	0.530	0.366–0.689	100.00	30.00	0.8006
rNOE*	0.514	0.270–0.758	20.00	100.00	0.9155

ROC, receiver operating characteristic; CEST, chemical exchange saturation transfer; MRI, magnetic resonance imaging; AKI, acute kidney injury; AUC, area under the ROC curve; CI, confidence interval; CO, cortex; MTR, magnetization transfer ratio; MTR_{asym}, asymmetric MTR; APT*, apparent amide proton transfer; rNOE*, apparent relayed nuclear Overhauser enhancement; OSOM, outer stripe of outer medulla; ISOM, inner stripe of outer medulla; IM + P, inner medulla and pelvis.

established method for studying the pathogenesis of AKI caused by RM. In this model, an intramuscular glycerol injection was used to induce reproducible renal lesions (46). The intramuscular injection of glycerol (47) results in myoglobin release into blood. After glomerular filtration, the concentration of myoglobin in the tubules results in tubular obstruction, and the consequent increase in intrarenal pressure compresses intrarenal blood vessels, leading to renal tissue ischemia. This is aggravated by the vasoconstrictive effects of myoglobin. The model's appearance, distribution, and reversibility are similar to the clinical RM phenomenon, in particular, the lesions observed in humans in the case of acute renal failure owing to crush injury (48). Therefore, we inferred that endogenous CEST would be helpful for the assessment of comparable renal pathologies as caused by allogeneic transfusion and crush syndrome in humans (46).

Limitations

There are several limitations of this study. First, AKI model was induced only in male mice by a single specific injection of glycerol. Although the gender and the dose were consistent with previously reported values in the literature (49,50), experiments with different doses of both genders could have been conducted to evaluate the feasibility of using CEST-MRI for the assessment of AKI severity. Second, the change in the CEST-MRI

signals associated with injury was related to edema, pH changes, apoptosis, and changes in blood flow. However, corresponding validation examinations based on terminal deoxynucleotidyl transferase deoxyuridine triphosphate (dUTP) nick end labeling (TUNEL) staining and dynamic contrast-enhanced MRI were not performed (51,52). Third, only semi-quantitative CEST analysis was performed in this study. Quantitative CEST (53,54) may provide more details on the biochemical basis of alterations. For example, fractional concentration can be used as a parameter for metabolic information, and the exchange rate can be used as a parameter associated with pH value (55). Finally, no other MRI-based contrasts [such as T1, T2, T1rho, diffusion-weighted imaging (DWI), diffusion tensor imaging (DTI), etc.] was examined and compared with the CEST analysis. It has been discussed in the literature that the CEST approaches might not have shown pure CEST effect, but rather water relaxation shine-through effects (56).

Conclusions

Longitudinally CEST-MRI in a mouse model of RM-induced AKI revealed that the MTR metric is sensitive to pathophysiological changes associated with RM-induced renal injury in the acute stage and its gradual recovery. The APT and rNOE effects at ±3.6 ppm are related to pathological changes in RM-induced AKI. The MTR value obtained from CEST-MRI can potentially be used to assess renal injury in RM.

Acknowledgments

Funding: This work was supported by the National Natural Science Foundation of China (No. U21A6005), Key-Area Research and Development Program of Guangdong Province (Nos. 2018B030340001 and 2018B030333001), and Guangdong Basic and Applied Basic Research Foundation (Nos. 2020A1515110577 and 2019A1515111182).

Footnote

Conflicts of Interest: All authors have completed the ICMJE uniform disclosure form (available at https://qims.amegroups.com/article/view/10.21037/qims-23-699/coif). The authors have no conflicts of interest to declare.

Ethical Statement: The authors are accountable for all aspects of the work in ensuring that questions related to the accuracy or integrity of any part of the work are appropriately investigated and resolved. Experiments were performed under a project license (No. 2016-0167) granted by Institutional Animal Care and Use Committee of Southern Medical University, in compliance with Southern Medical University institutional guidelines for the care and use of animals.

References

1. Vanholder R, Sever MS, Erek E, Lameire N. Rhabdomyolysis. J Am Soc Nephrol 2000;11:1553-61.
2. Fähling M, Mathia S, Paliege A, Koesters R, Mrowka R, Peters H, Persson PB, Neumayer HH, Bachmann S, Rosenberger C. Tubular von Hippel-Lindau knockout protects against rhabdomyolysis-induced AKI. J Am Soc Nephrol 2013;24:1806-19.
3. Heard H, Barker J. Recognizing, diagnosing, and treating rhabdomyolysis. JAAPA 2016;29:29-32.
4. Harrois A, Libert N, Duranteau J. Acute kidney injury in trauma patients. Curr Opin Crit Care 2017;23:447-56.
5. Ward MM. Factors predictive of acute renal failure in rhabdomyolysis. Arch Intern Med 1988;148:1553-7.
6. Hoste EAJ, Kellum JA, Selby NM, Zarbock A, Palevsky PM, Bagshaw SM, Goldstein SL, Cerdá J, Chawla LS. Global epidemiology and outcomes of acute kidney injury. Nat Rev Nephrol 2018;14:607-25.
7. Simpson JP, Taylor A, Sudhan N, Menon DK, Lavinio A. Rhabdomyolysis and acute kidney injury: creatine kinase as a prognostic marker and validation of the McMahon Score in a 10-year cohort: A retrospective observational evaluation. Eur J Anaesthesiol 2016;33:906-12.
8. Singh R, Dodkins J, Doyle JF, Forni LG. Acute Kidney Injury Biomarkers: What Do They Tell Us? Contrib Nephrol 2018;193:21-34.
9. Waikar SS, Betensky RA, Emerson SC, Bonventre JV. Imperfect gold standards for kidney injury biomarker evaluation. J Am Soc Nephrol 2012;23:13-21.

10. Bagshaw SM, Bellomo R, Devarajan P, Johnson C, Karvellas CJ, Kutsiogiannis DJ, Mehta R, Pannu N, Romanovsky A, Sheinfeld G, Taylor S, Zappitelli M, Gibney RT. Review article: Renal support in critical illness. Can J Anaesth 2010;57:999-1013.
11. Moinuddin I, Bracamonte E, Thajudeen B, Sussman A, Madhrira M, Costello J. Allergic Interstitial Nephritis Manifesting as a Striated Nephrogram. Case Rep Med 2015;2015:250530.
12. Mahmoud H, Buchanan C, Francis ST, Selby NM. Imaging the kidney using magnetic resonance techniques: structure to function. Curr Opin Nephrol Hypertens 2016;25:487-93.
13. Michielsen K, Meersschaert J, De Keyzer F, Cannie M, Deprest J, Claus F. MR volumetry of the normal fetal kidney: reference values. Prenat Diagn 2010;30:1044-8.
14. Dekkers IA, Lamb HJ. Clinical application and technical considerations of T(1) & T(2)(*) mapping in cardiac, liver, and renal imaging. Br J Radiol 2018;91:20170825.
15. Prasad PV, Edelman RR, Epstein FH. Noninvasive evaluation of intrarenal oxygenation with BOLD MRI. Circulation 1996;94:3271-5.
16. Inoue T, Kozawa E, Okada H, Inukai K, Watanabe S, Kikuta T, Watanabe Y, Takenaka T, Katayama S, Tanaka J, Suzuki H. Noninvasive evaluation of kidney hypoxia and fibrosis using magnetic resonance imaging. J Am Soc Nephrol 2011;22:1429-34.
17. Maekawa M, Imaizumi T, Yamakawa T, Ito Y. Acute Renal Failure with Severe Loin Pain and Patchy Renal Vasoconstriction in a Patient without Hypouricemia, Provoked by Epileptic Seizure. Intern Med 2017;56:2001-5.
18. Caroli A, Schneider M, Friedli I, Ljimani A, De Seigneux S, Boor P, Gullapudi L, Kazmi I, Mendichovszky IA, Notohamiprodjo M, Selby NM, Thoeny HC, Grenier N, Vallée JP. Diffusion-weighted magnetic resonance imaging to assess diffuse renal pathology: a systematic review and statement paper. Nephrol Dial Transplant 2018;33:ii29-40.
19. Hernandez-Garcia L, Lahiri A, Schollenberger J. Recent progress in ASL. Neuroimage 2019;187:3-16.
20. Selby NM, Williams JP, Phillips BE. Application of dynamic contrast enhanced ultrasound in the assessment of kidney diseases. Curr Opin Nephrol Hypertens 2021;30:138-43.
21. Tao Q, Zhang D, Zhang Q, Liu C, Ye S, Feng Y, Liu R. Mitochondrial targeted ROS scavenger based on nitroxide for treatment and MRI imaging of acute kidney injury. Free Radic Res 2022;56:303-15.
22. Ward KM, Aletras AH, Balaban RS. A new class of contrast agents for MRI based on proton chemical exchange dependent saturation transfer (CEST). J Magn Reson 2000;143:79-87.
23. van Zijl PC, Yadav NN. Chemical exchange saturation transfer (CEST): what is in a name and what isn't? Magn Reson Med 2011;65:927-48.
24. Longo DL, Irrera P, Consolino L, Sun PZ, McMahon MT. Renal pH Imaging Using Chemical Exchange Saturation Transfer (CEST) MRI: Basic Concept. Methods Mol Biol 2021;2216:241-56.
25. Tao Q, Yi P, Cai Z, Chen Z, Deng Z, Liu R, Feng Y. Ratiometric chemical exchange saturation transfer pH mapping using two iodinated agents with nonequivalent amide protons and a single low saturation power. Quant Imaging Med Surg 2022;12:3889-902.
26. Longo DL, Busato A, Lanzardo S, Antico F, Aime S. Imaging the pH evolution of an acute kidney injury model by means of iopamidol, a MRI-CEST pH-responsive contrast agent. Magn Reson Med 2013;70:859-64.
27. Irrera P, Consolino L, Cutrin JC, Zöllner FG, Longo DL. Dual assessment of kidney perfusion and pH by exploiting a dynamic CEST-MRI approach in an acute kidney ischemia-reperfusion injury murine model. NMR Biomed 2020;33:e4287.
28. Stabinska J, Singh A, Haney NM, Li Y, Sedaghat F, Kates M, McMahon MT. Noninvasive assessment of renal dynamics and pH in a unilateral ureter obstruction model using DCE MR-CEST urography. Magn Reson Med 2023;89:343-55.
29. Wang F, Kopylov D, Zu Z, Takahashi K, Wang S, Quarles CC, Gore JC, Harris RC, Takahashi T. Mapping murine diabetic kidney disease using chemical exchange saturation transfer MRI. Magn Reson Med 2016;76:1531-41.
30. Liu J, Han Z, Chen G, Li Y, Zhang J, Xu J, van Zijl PCM, Zhang S, Liu G. CEST MRI of sepsis-induced acute kidney injury. NMR Biomed 2018;31:e3942.
31. Kim M, Gillen J, Landman BA, Zhou J, van Zijl PC. Water saturation shift referencing (WASSR) for chemical exchange saturation transfer (CEST) experiments. Magn Reson Med 2009;61:1441-50.
32. Yang L, Ding Y, Rao S, Chen C, Zeng M. T(1) Mapping on Gd-EOB-DTPA-Enhanced MRI for the Prediction of Oxaliplatin-Induced Liver Injury in a Mouse Model. J Magn Reson Imaging 2021;53:896-902.
33. Fluss R, Faraggi D, Reiser B. Estimation of the

Youden Index and its associated cutoff point. Biom J 2005;47:458-72.
34. Zhou J, Heo HY, Knutsson L, van Zijl PCM, Jiang S. APT-weighted MRI: Techniques, current neuro applications, and challenging issues. J Magn Reson Imaging 2019;50:347-64.
35. Shah SM, Mougin OE, Carradus AJ, Geades N, Dury R, Morley W, Gowland PA. The z-spectrum from human blood at 7T. Neuroimage 2018;167:31-40.
36. Panizo N, Rubio-Navarro A, Amaro-Villalobos JM, Egido J, Moreno JA. Molecular Mechanisms and Novel Therapeutic Approaches to Rhabdomyolysis-Induced Acute Kidney Injury. Kidney Blood Press Res 2015;40:520-32.
37. Manis T, George-Varghese B, Kashani J. Rhabdomyolysis - Go big or go home. Am J Emerg Med 2019;37:2194-6.
38. Zhou Y, Bie C, van Zijl PCM, Yadav NN. The relayed nuclear Overhauser effect in magnetization transfer and chemical exchange saturation transfer MRI. NMR Biomed 2023;36:e4778.
39. Desmond KL, Moosvi F, Stanisz GJ. Mapping of amide, amine, and aliphatic peaks in the CEST spectra of murine xenografts at 7 T. Magn Reson Med 2014;71:1841-53.
40. Zhang XY, Wang F, Afzal A, Xu J, Gore JC, Gochberg DF, Zu Z. A new NOE-mediated MT signal at around -1.6ppm for detecting ischemic stroke in rat brain. Magn Reson Imaging 2016;34:1100-6.
41. Zu Z, Lin EC, Louie EA, Xu J, Li H, Xie J, Lankford CL, Chekmenev EY, Swanson SD, Does MD, Gore JC, Gochberg DF. Relayed nuclear Overhauser enhancement sensitivity to membrane Cho phospholipids. Magn Reson Med 2020;84:1961-76.
42. Zhou J, Wilson DA, Sun PZ, Klaus JA, Van Zijl PC. Quantitative description of proton exchange processes between water and endogenous and exogenous agents for WEX, CEST, and APT experiments. Magn Reson Med 2004;51:945-52.
43. Zu Z, Li H, Xu J, Zhang XY, Zaiss M, Li K, Does MD, Gore JC, Gochberg DF. Measurement of APT using a combined CERT-AREX approach with varying duty cycles. Magn Reson Imaging 2017;42:22-31.
44. Kim B, Schär M, Park H, Heo HY. A deep learning approach for magnetization transfer contrast MR fingerprinting and chemical exchange saturation transfer imaging. Neuroimage 2020;221:117165.
45. Jiang K, Ferguson CM, Woollard JR, Zhu X, Lerman LO. Magnetization Transfer Magnetic Resonance Imaging Noninvasively Detects Renal Fibrosis in Swine Atherosclerotic Renal Artery Stenosis at 3.0 T. Invest Radiol 2017;52:686-92.
46. Tonnus W, Al-Mekhlafi M, Hugo C, Linkermann A. Assessment of In vivo Kidney Cell Death: Acute Kidney Injury. Methods Mol Biol 2018;1857:135-44.
47. Wang S, Zhang C, Li J, Niyazi S, Zheng L, Xu M, Rong R, Yang C, Zhu T. Erythropoietin protects against rhabdomyolysis-induced acute kidney injury by modulating macrophage polarization. Cell Death Dis 2017;8:e2725.
48. Finckh ES. The indirect action of subcutaneous injections of glycerol on the renal tubules in the rat. J Pathol Bacteriol 1959;78:197-202.
49. Zhou J, Bai Y, Jiang Y, Tarun P, Feng Y, Huang R, Fu P. Immunomodulatory role of recombinant human erythropoietin in acute kidney injury induced by crush syndrome via inhibition of the TLR4/NF-κB signaling pathway in macrophages. Immunopharmacol Immunotoxicol 2020;42:37-47.
50. Yuqiang C, Lisha Z, Jiejun W, Qin X, Niansong W. Pifithrin-α ameliorates glycerol induced rhabdomyolysis and acute kidney injury by reducing p53 activation. Ren Fail 2022;44:473-81.
51. Wang F, Jiang RT, Tantawy MN, Borza DB, Takahashi K, Gore JC, Harris RC, Takahashi T, Quarles CC. Repeatability and sensitivity of high resolution blood volume mapping in mouse kidney disease. J Magn Reson Imaging 2014;39:866-71.
52. Wu CJ, Bao ML, Wang Q, Wang XN, Liu XS, Shi HB, Zhang YD. Acute kidney damage induced by low- and iso-osmolar contrast media in rats: Comparison study with physiologic MRI and histologic-gene examination. J Magn Reson Imaging 2017;45:291-302.
53. Ji Y, Zhou IY, Qiu B, Sun PZ. Progress toward quantitative in vivo chemical exchange saturation transfer (CEST) MRI. Isr J Chem 2017;57:809-24.
54. Zhao Y, Wang X, Wang Y, Wang B, Zhang L, Wei X, He X. Application of a Markov chain Monte Carlo method for robust quantification in chemical exchange saturation transfer magnetic resonance imaging. Quant Imaging Med Surg 2022;12:5140-55.
55. Wu R, Xiao G, Zhou IY, Ran C, Sun PZ. Quantitative chemical exchange saturation transfer (qCEST) MRI - omega plot analysis of RF-spillover-corrected inverse CEST ratio asymmetry for simultaneous determination of labile proton ratio and exchange rate. NMR Biomed 2015;28:376-83.
56. Zaiss M, Windschuh J, Paech D, Meissner JE, Burth

S, Schmitt B, Kickingereder P, Wiestler B, Wick W, Bendszus M, Schlemmer HP, Ladd ME, Bachert P, Radbruch A. Relaxation-compensated CEST-MRI of the human brain at 7T: Unbiased insight into NOE and amide signal changes in human glioblastoma. Neuroimage 2015;112:180-8.

Cite this article as: Zhang Q, Tao Q, Xie Y, Chen Z, Seeliger E, Niendorf T, Chen W, Feng Y. Assessment of rhabdomyolysis-induced acute kidney injury with chemical exchange saturation transfer magnetic resonance imaging. Quant Imaging Med Surg 2023;13(12):8336-8349. doi: 10.21037/qims-23-699

